Proceedings of the Institute of Acoustics

SONAR SENSITIVITY TO SCINTILLATING SOUND SIGNALS IN THE SEA

PF Dobbins British Aerospace, Land & Sea Systems, PO Box 5, Filton, Bristol BS34 7QW

1. INTRODUCTION

In underwater acoustics, signal fluctuations are caused by internal waves, turbulence, and other oceanographic phenomena, as well as multi-path propagation and scattering from the surface and bottom. These fluctuations impose a limit on the performance of sonar and other underwater systems. The amplitude fluctuations bring about signal fading and the failure to detect targets well within the theoretical range of the sonar. This is referred to as scintillation in astronomy or, more colloquially, twinkling stars. Phase fluctuations cause a loss of directivity or angular resolution of receiving arrays, spreading of transmitted beams, variations in the apparent arrival direction of signals and uncertainty in their arrival time. These effects have much in common with the shimmering of objects seen through a heat-haze.

The causes of fluctuations and their effects on wave propagation have been the subject of much research in the fields of sonar, radar, astronomy and laser propagation. In underwater acoustics the existence of fluctuation phenomena has been demonstrated experimentally for a variety of causes [1, 2, 3, 4, 5, 6]. The resulting degradation of system performance, however, and means of overcoming it, have received much less attention. Probably the most significant problems are loss of gain and angular resolution [7]. Fluctuations limit the directivity of an array, which means that there is a maximum useful size for an array in any particular environment - generally about 50-100 wavelengths [7], giving 0.5-1.0° angular resolution. Without compensating for the fluctuations in the wavefield or other special processing, no increase in gain or angular discrimination can be obtained by making the array larger.

Previous papers have presented numerical simulations of these phenomena [8] and theoretical predictions of the directivity pattern of an array subject to correlated phase and amplitude fluctuations [9]. The present paper compares these predictions with recent experimental results from sea-going trials with a very long towed array.

2. THEORETICAL BACKGROUND

2.1 Acoustic Fluctuations

No attempt will be made here to model the acoustic propagation effects that result in fluctuating signals. These effects are reasonably well understood for individual isolated scattering mechanisms, such as rough sea beds or internal waves, but the experimental signals that will be examined below exhibit the combined effects of surface scattering, bottom scattering, volume fluctuations and multipaths. These various contributions have not yet been unravelled so, instead, the statistical description of the fluctuating wavefield, required for beamforming predictions, will be derived empirically directly from the received signals.

The most relevant descriptor is the spatially dependent mutual coherence function. However, it is more convenient to measure the phase and amplitude of the array signals, and the coherence function may be obtained from these using the following relationship [10]:

$$\Gamma(r) = \exp\left[< S^2 > \{C_S(r)-1\} + < \chi^2 > \{C_\chi(r)-1\} \right] \quad (1)$$

where $\Gamma(r)$ is the coherence function, r is spatial separation, S is phase, χ is the natural log of amplitude, $<S^2>$ and $<\chi^2>$ are the variances of phase and log-amplitude, and $C_S(r)$ and $C_\chi(r)$ are the spatial correlation functions for phase and log-amplitude fluctuations.

It is also informative to consider the fluctuating wavefront as made up of a spectrum of plane waves travelling in different directions. The spread of this angular spectrum ultimately determines the directivity achievable from an array, as will be discussed in the following Section. However, the angular spectrum is directly related to the spatial coherence function by a Fourier transform. Because of this, it is convenient to use the more easily obtained coherence function in theoretical descriptions of the beamforming process.

2.2 Beamforming

It is anticipated that the array beampattern will be distorted by fluctuations in the incident wavefield, and that this distorted beampattern will vary with time as the signals change. Realisations of the pattern at an instant in time can be produced using numerical simulations [7, 8], but in practical sonar systems it is the average directivity over a period comparable with the integration time or the length of transmitted pulses that is of interest.

The expected average beampattern for an arbitrary array with any geometry, shading or steering can be found by convolving the error-free beampattern with the angular spectrum of the incident fluctuating wavefield [7]. However, for the specific case of a uniformly spaced, unshaded and unsteered line array, this convolution leads to a simple analytical formula expressed in terms of the mutual coherence function [7, 9]:

$$\left\langle B(\theta)^2 \right\rangle = \frac{2}{N^2}\left\{ \frac{N}{2} + \sum_{n=1}^{N-1} (N-n)\Gamma(nd)\cos(nkd\sin\theta) \right\} \quad (2)$$

where $<B(\theta)^2>$ is the mean square beampattern (or average power beampattern), θ is azimuth bearing, N is the number of hydrophone elements in the array, d is the element spacing, and k is the wavenumber ($k = 2\pi f/\lambda$).

3. THE EXPERIMENT

A series of sea trials were carried out in the Tyrrhenian Sea during September and October 1998. In the experimental runs considered here, broadband acoustic signals were generated by small explosive charges, detonated at depths of about 10 m. These signals were recorded by a hydrophone array, at distances of up to 46 km from the source. This array was a horizontal towed array consisting of up to 660 hydrophones with a regular spacing, and towed at depths between 70 and 400 m.

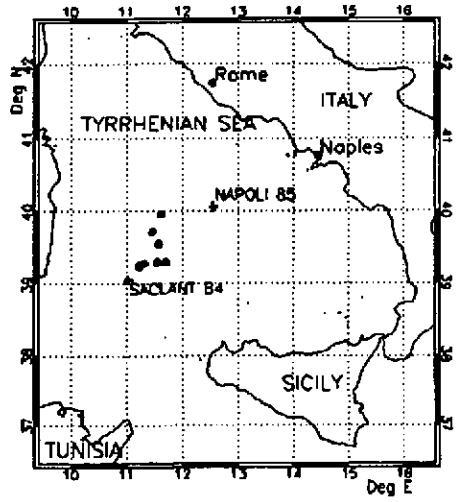

Fig. 1 Map of Tyrrhenian Sea showing location of present experiments (solid circles) as well as NAPOLI 85 [12] and SACLANT 84 [11] (crosses).

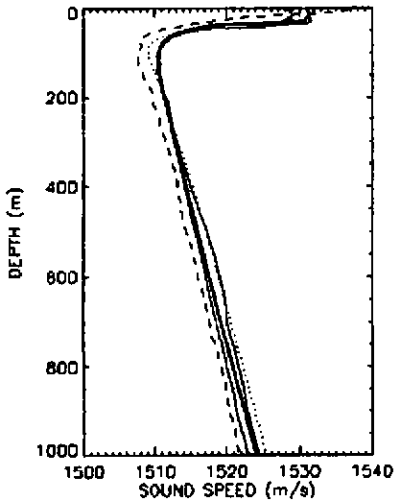

Fig. 2 Sound speed profiles from present experiments (solid lines) compared with profiles from SACLANT 84 (dots) and NAPOLI 85 (dashes).

A total of 54 detonations relevant to this study were carried out over a period of seven days. Additionally, oceanographic observations were made with regular XBT casts. These were used to determine the sound-speed profile, allowing estimates to be made of the propagation paths between source and receiver.

3.1 The Location

The Tyrrhenian Sea is one of the major basins of the Mediterranean Sea, and is connected to the Mediterranean via the large Sardinia-Sicily Channel. The experimental site was in the central Tyrrhenian Sea, where the water depth was in the order of 3000 m. A map of the area is shown in Fig. 1. The locations of receive array at the start of each run are marked as solid circles.

For reference, the locations of two other relevant experiments previously conducted in the area at the same time of year are also shown. These are an oceanographic survey carried out by SACLANT in 1984 [11], referred to here as SACLANT 84, and the NAPOLI 85 experiment carried out by SACLANT and Cambridge University in 1985 [12].

3.2 Propagation Conditions

Typical sound speed profiles from the present experiments are shown as the solid lines in Fig. 2, along with profiles from SACLANT 84 and NAPOLI 85, shown as dots and dashes respectively. It will be seen that the overall shape of these profiles is remarkably stable over several years. However, there are also variations in detail over the short period of these experiments. It is also clear that there is a strong surface duct extending down to about 50 m depth.

Because of the shallow depth of the sources used in these experiments, the surface duct trapped sound propagating near the horizontal and in many runs there was no direct path between source and receiver. In these cases, the received signals were composed entirely of surface or bottom reflections. However, at the maximum range of 46 km, direct paths were available and these are the

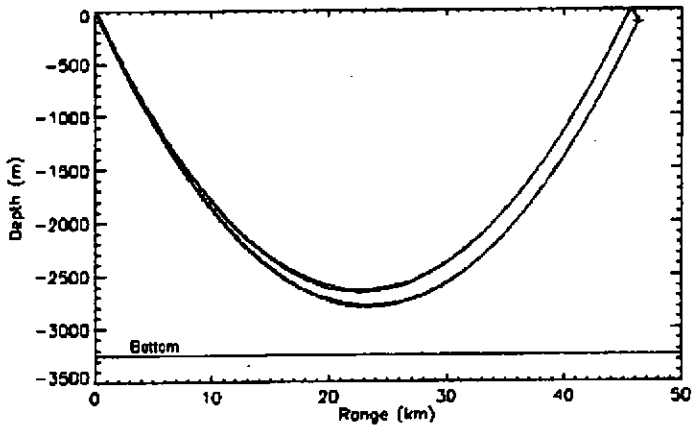

Fig. 3 Predicted paths for source at 10 m depth and receiver at 120 m depth, 46 km range.

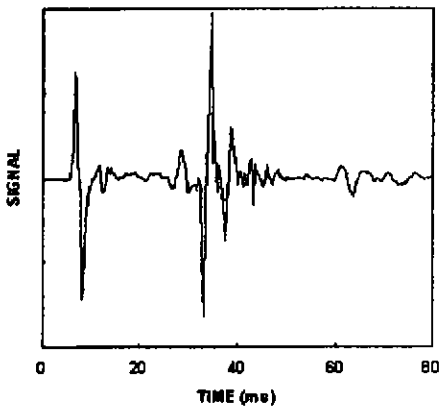

Fig. 4 Initial impulse and reflections at receiver in Fig. 3.

signals used in the following analysis. A typical group of raypaths from a source at 10 m depth to a receiver at 120 m is shown in Fig. 3.

A close inspection of the two major rays in Fig. 3 reveals that each actually comprises two rays – one radiating directly from the source and one reflected from the surface above. Thus, a direct signal and three reflections are anticipated, predicted to follow at 2, 32 and 34 ms. This is clearly visible in the received signal shown in Fig. 4. Other paths via bottom reflections exist, but they arrive much later and can be neglected for now.

3.3 The Signals

The explosive signals used in these experiments are broadband in nature, but for initial investigations of beamforming performance, phase and amplitude variations along the array at specific frequencies were required. If $E_n(t)$ is the field measured at the nth hydrophone, the frequency content of the signal is given by its Fourier transform, $\hat{E}_n(\omega)$. A simple estimate of the relative variations in the field along the array is found by selecting the signal from one element as a reference, $E_R(t)$ (no recordings of the transmitted signals were made), and then forming the ratio

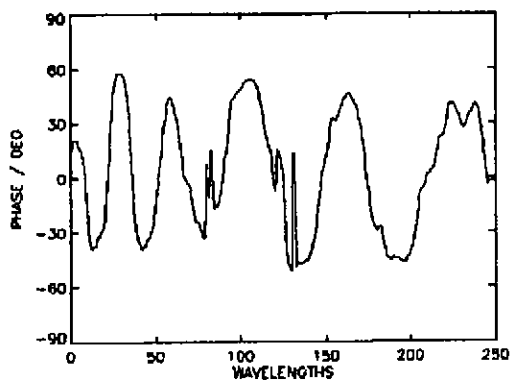

Fig. 5 Phase plotted against distance along array for propagation paths in Fig. 3 at nominal operating frequency.

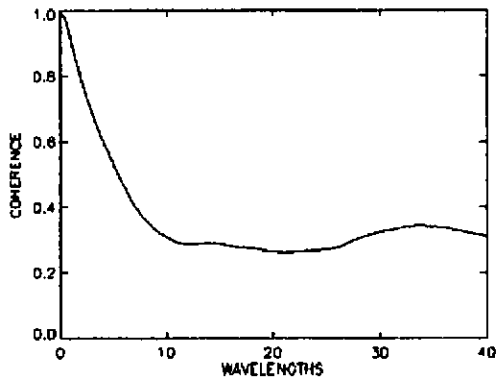

Fig. 6 Mutual coherence function computed from data corresponding to Fig. 5.

$$\hat{R}_n(\omega) = \hat{E}_n(\omega)/\hat{E}_R(\omega) \quad (3)$$

where $\hat{R}_n(\omega)$ is the relative frequency response at the nth hydrophone. This approach is subject to limitations, especially where the reference passes through zero, but does provide useful preliminary information.

Typical phase variations at the nominal array operating frequency are plotted against distance along the array in wavelengths in Fig. 5. This example is for the propagation paths shown in Fig. 3, but it should be pointed out that it may also include errors due to the array shape deviating from a straight line. The corresponding coherence function, from Eq.(1), is shown in Fig. 6. It may be seen that the coherence scale is in the order of ten wavelengths. This is shorter than expected for direct path propagation, but compares with values in the range of 10 – 50 λ previously observed under multipath conditions [13].

4. BEAMFORMING PERFORMANCE

The data described above may be used to compute realisations of the beampattern for comparison with the theoretical average pattern given by Eq.(2). The ideal pattern, in the absence of fluctuations, for an unshaded uniform line array is given by the conventional beamforming formula:

$$B_{Ideal}(\theta) = \frac{1}{N}\left|\sum_{n=1}^{N}\exp\{i(nkd\sin\theta)\}\right| \quad (4)$$

and the amplitude and phase fluctuations for a single realisation can be included by a simple modification:

$$B_{Fluctations}(\theta) = \frac{1}{N}\left|\sum_{n=1}^{N}A_n\exp\{i(nkd\sin\theta - \phi_n)\}\right| \quad (5)$$

where A_n is the amplitude at the nth element and ϕ_n is the phase.

The plots in the left hand column in Fig. 7 show the first 10 realisations using this formula, combined with the experimental data described above, for arrays of 8 (top), 24 (middle) and 72 (bottom) wavelengths. Note the changing scale on the x-axis. The peak level in these plots has been normalised to remove the large amplitude variations. Nevertheless, the developing character of the beampattern degradation is clearly visible as the array aperture is increased from just less than the coherence length to several times the coherence length.

In the right hand column the average pattern computed from 100 realisations is plotted as a dashed line, compared with the theoretical average from Eq.(2) as the solid line and, for completeness, the error-free pattern shown as a dotted line.

Again, the changing effects as the array length is increased are obvious. Where the array is shorter than the coherence scale, there is some filling in between sidelobes in the average patterns, but overall the degradation is not serious. The realisations on the left show that, generally, the instantaneous pattern does not differ greatly from the ideal, but occasionally the sidelobe levels are raised or the main beam is broadened. This is presumably caused by some transient feature in the fluctuating wavefield.

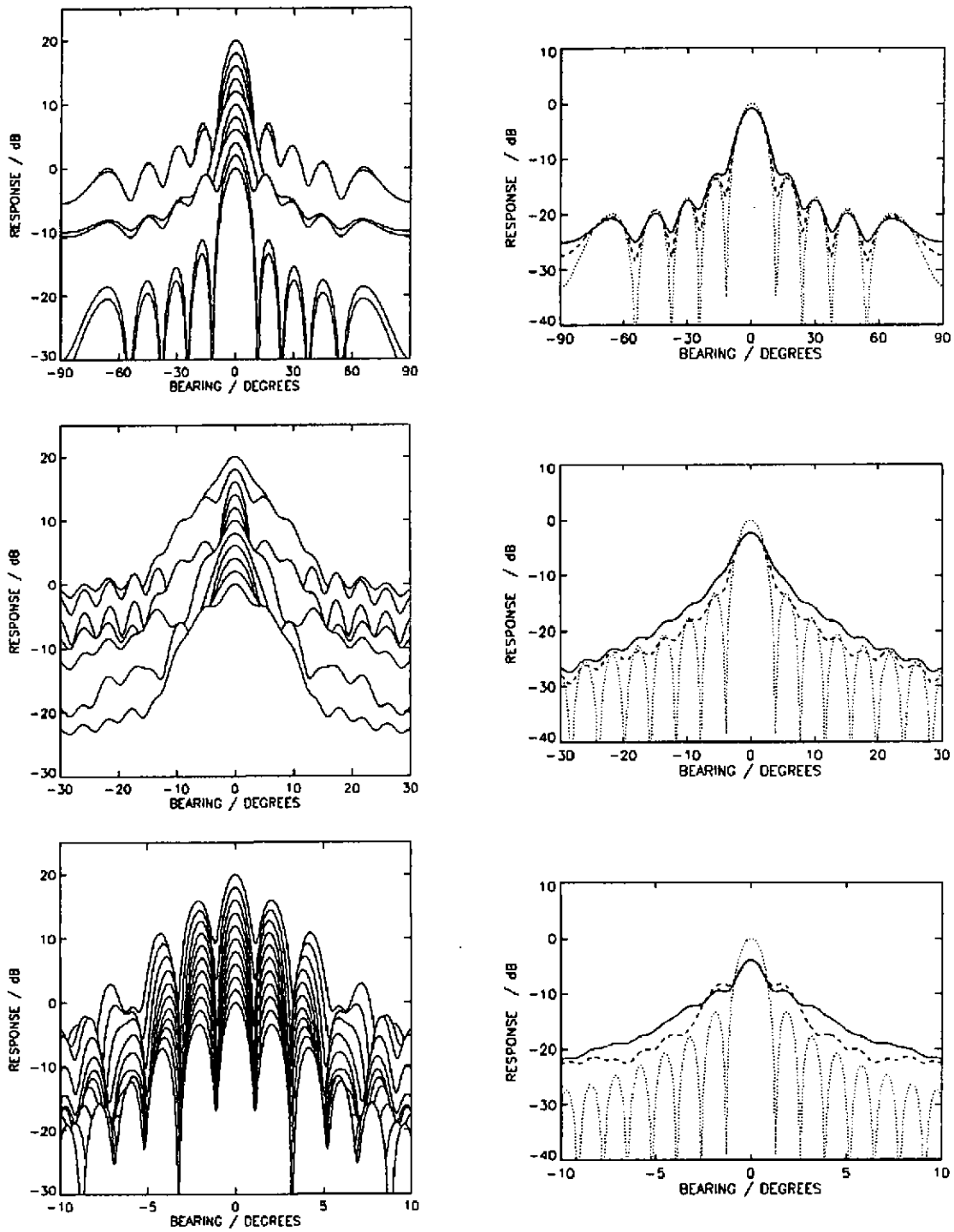

Fig. 7 Left hand column shows first 10 realisations of beampattern for arrays of 8 (top), 24 (middle) and 72λ (bottom), and right hand column shows corresponding average patterns (dashed lines) compared with ideal pattern (dots) and theoretical average (solid).

Where the array is a little larger than the coherence scale, the realisations show several seriously distorted patterns and the averages more or less follow the envelope of the sidelobes in the ideal pattern, with a slight drop in main beam sensitivity.

In the third case, where the array is much longer than the coherence scale, individual realisations show little variation, at least close to the main beam, but sidelobes are raised significantly. Now the averages show a drop of several dB in main beam sensitivity and the broadened patterns fall away much more slowly than the sidelobes in the ideal pattern. This would obviously represent a considerably reduced DI.

Finally, it is seen in each of these example cases that the theoretical average pattern is in reasonable agreement with the averages computed from the data. The theoretical average does tend to exaggerate the pattern degradation slightly. The reason for this is not yet known, but overall the theoretical average does give a very good indication of the form of the average pattern derived from experiment.

5. DISCUSSION AND CONCLUSIONS

A preliminary analysis of recently acquired experimental data has been presented, and the effect of acoustic fluctuations on beampatterns compared with the predictions of a previously published theory [7, 9].

Generally, the results are encouraging. The theoretical average patterns shown in the right hand column of Fig. 7 are in good agreement with the averages computed from the data, although it can be seen on close inspection that there is a slight tendency for the theory to over-exaggerate the degradation of the pattern.

Nevertheless, there are some aspects of these results that warrant further investigation. The first of these is apparent in the bottom left hand plot Fig. 7. The similarity between the patterns suggests that the phase and amplitude data used for successive realisations may not have been independent. If this is the case, a closer examination of the signal coherence in time and frequency as well as space will allow more appropriate selection of data samples for the realisations.

The other area of concern is the use of signals that exhibit the combined effects of surface scattering, bottom scattering, volume fluctuations and multipaths. This in no way invalidates the findings presented here, but does mean that it is difficult to extrapolate from these results to other situations.

However, one of the long term aims of this research is to determine just what is the ultimate limit on sonar array size due to environmental phenomena and, perhaps more importantly, what can be done to overcome the problem. As already stated, the agreement between theory and experiment found here is encouraging. This suggests that the theory may be used with confidence in predicting this ultimate limit in any case where the spatial coherence function is known, whether the precise mechanism causing loss of coherence is understood or not.

6. ACKNOWLEDGEMENT

This work has been carried out with the support of DERA, Winfrith under contract SSDW1/944.

7. REFERENCES

[1] D.E. Weston, A.A. Horrigan, S.J.L. Thomas and J. Revie, 'Studies of Sound Transmission Fluctuations in Shallow Coastal Waters', Phil. Trans. Roy. Soc. London, 265(1169), 567-608 (1969).

[2] G.C. Gaunaurd, *Categorized bibliography on the topic of underwater sound transmission fluctuations*, NOLTR 73-176, Naval Ordnance Lab., MD 20910, USA (1973).

[3] H.B. Ali, *Spatial and temporal variabilities in underwater acoustic transmission: an analytical review*, SACLANTCEN SM-166, SACLANT ASW Research Centre, La Spezia, Italy (1983).

[4] P.F. Dobbins, *Sonar Degradation due to Sea Water Inhomogeneity: A Review of Relevant Literature*, British Aerospace TR. 1384, May 1984.

[5] P.F. Dobbins, *A Literature Review on Fluctuations in Long Range Low Frequency Acoustic Propagation and Related Oceanographic Phenomena. Volume 1: The Review*, British Aerospace MNC 00127 Vol.1, June 1991.

[6] G. Kirby, *Environmental Uncertainty in Sonar Modelling*, BAeSEMA C2977/6/TR.4, September 1993.

[7] P.F. Dobbins, *Degradation of Coherence of Acoustic Signals Resulting from Inhomogeneities in the Sea*, PhD Thesis, University of Bath (1989).

[8] P.F. Dobbins and C. Schofield, 'Numerical Simulations of the Degradation of Array Directivity due to Scattering', *Proc. Inst. Acoust.*, 7(3), 67-75 (1985).

[9] P.F. Dobbins, 'Array directivity, sea water inhomogeneity and the plane wave spectrum', *Proc. Inst. Acoust.*, 12(1), 123-130 (1990).

[10] A. Ishimaru, *Wave Propagation and Scattering in Random Media*, Academic Press (1978).

[11] T.S. Hopkins & P. Zanasca, *Oceanographic data from the southern Tyrrhenian Sea: August-October 1984*, SACLANTCEN Memorandum No. SM-198, SACLANT Undersea Research Centre, La Spezia, Italy (1988).

[12] B.J. Uscinski, J.R. Potter and T. Akal, 'Broadband acoustic transmission fluctuations during NAPOLI 85, an experiment in the Tyrrhenian Sea: Preliminary results and an arrival-time analysis', *J. Acoust. Soc. Am.*, 86(2), 706-715 (1989).

[13] W.M. Carey, 'The determination of signal coherence length based on signal coherence and gain measurements in deep and shallow water', *J. Acoust. Soc. Am.*, 104(2), 831-837 (1998).